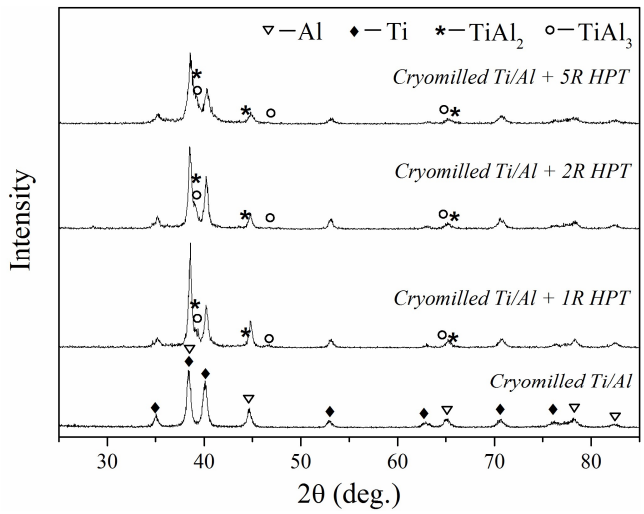

Figure 1. XRD profiles of the 10h cryomilled Ti/Al powder and the compacts that subsequently HPT deformed for 1, 2 and 5 revolutions.

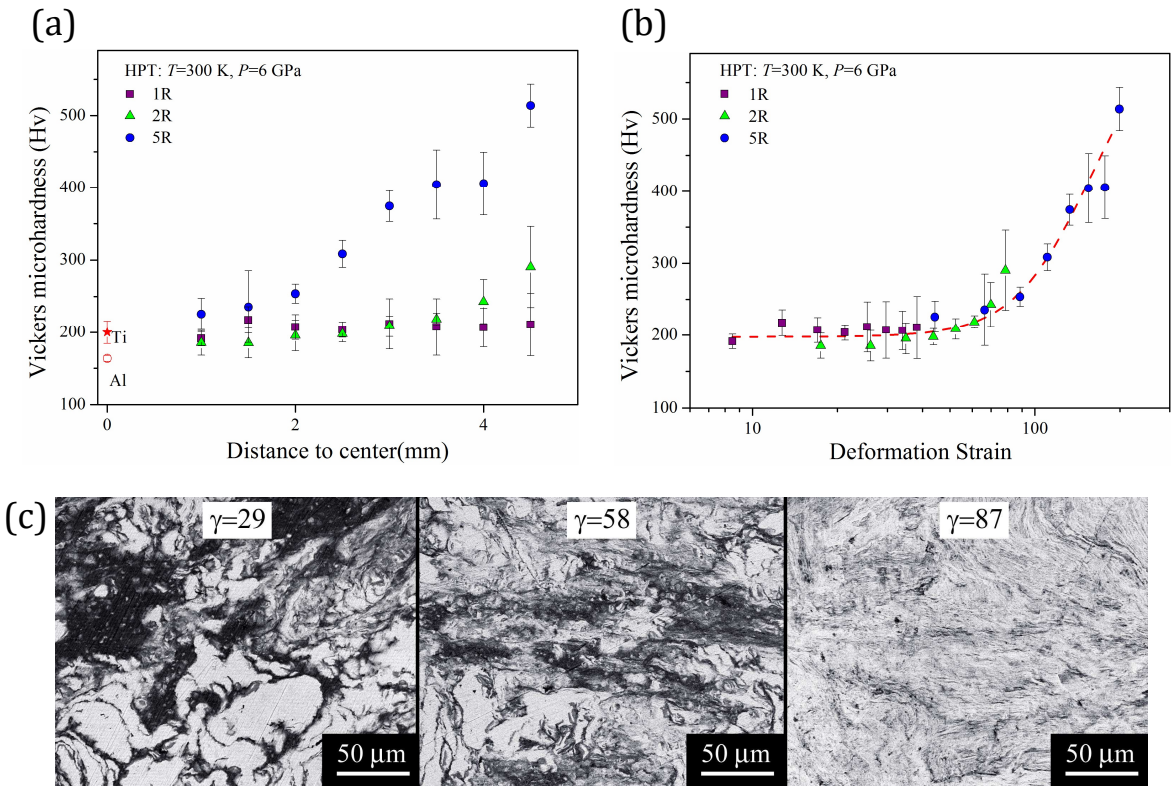

Figure 2. Vickers microhardness as function of distance to center (a) and HPT deformation strain (b) for 1, 2 and 5 revolutions HPT processed samples. (c) SEM micrographs of the locations with shear strain (γ) of 29, 58 and 87 in the 2 revolutions HPT deformed sample.

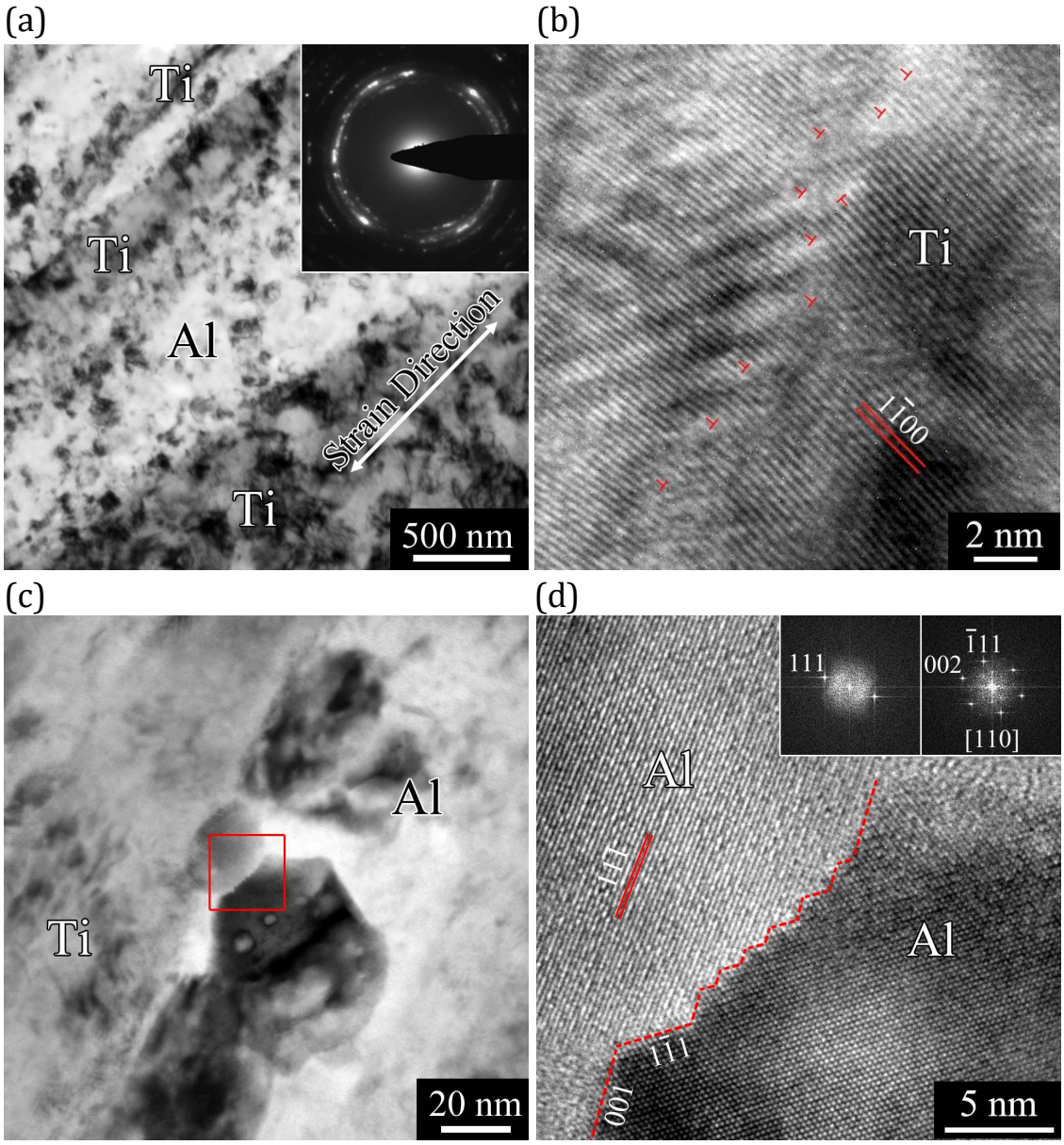

Figure 3. (a) Bright field TEM micrograph and the SAED pattern (inset) of the Al/Ti interface in the γ29 FIB lifted TEM sample. (b) Low-angle grain boundary formed in the Ti. (c) Bright field TEM micrograph of the Al grains along the Al/Ti interphase boundary in the γ29 sample. (d) HRTEM micrograph of the Al grain boundary marked by the box in Fig. 3c and the corresponding FFT patterns.

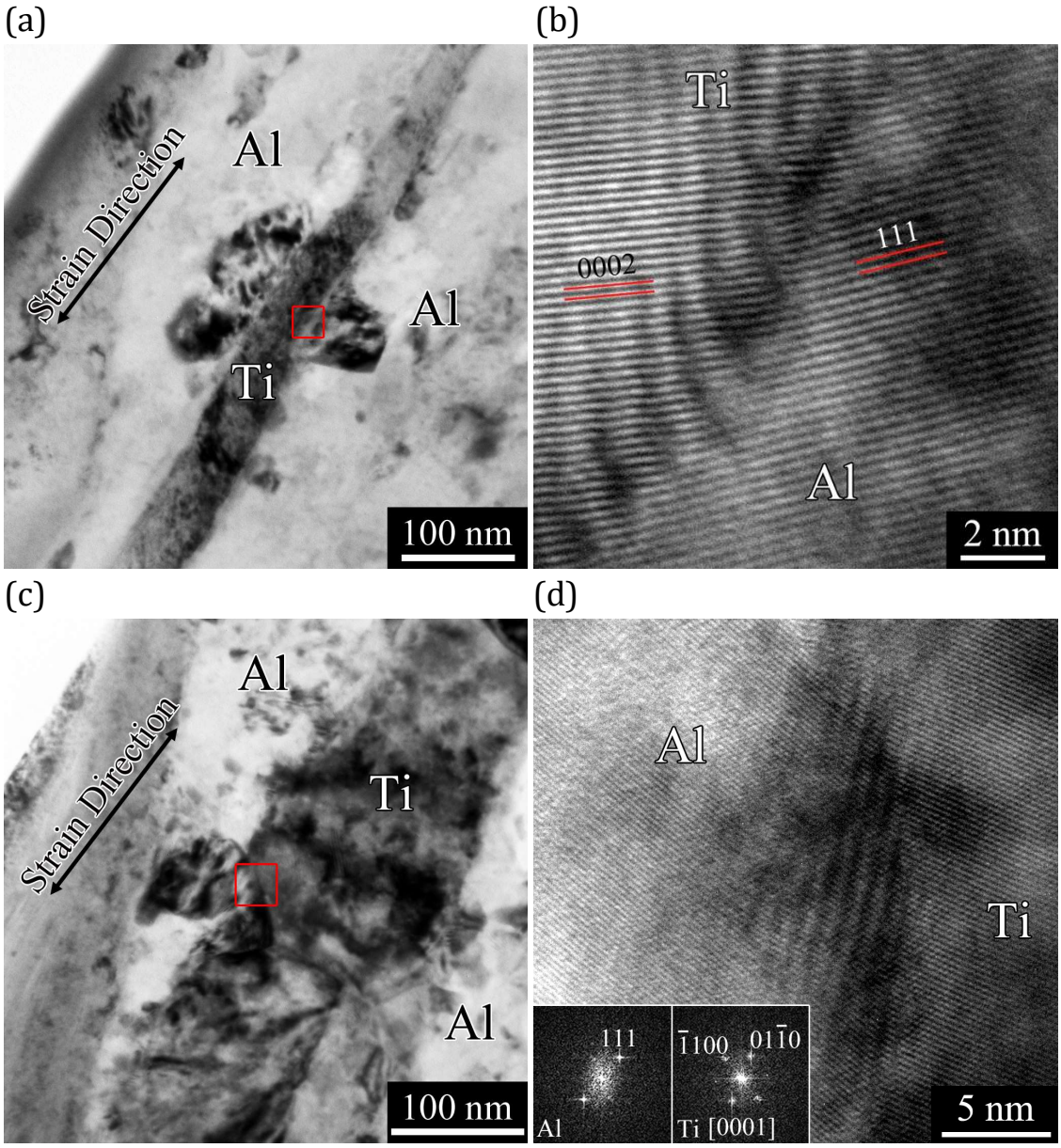

Figure 4. (a)Bright field TEM and (b) HRTEM micrographs of the semi-coherent Al/Ti interphase boundary in the γ29 sample. (c) Bright field TEM and (d) HRTEM micrographs of the incoherent Al/Ti interphase boundary in the γ29 sample and the corresponding FFT patterns.

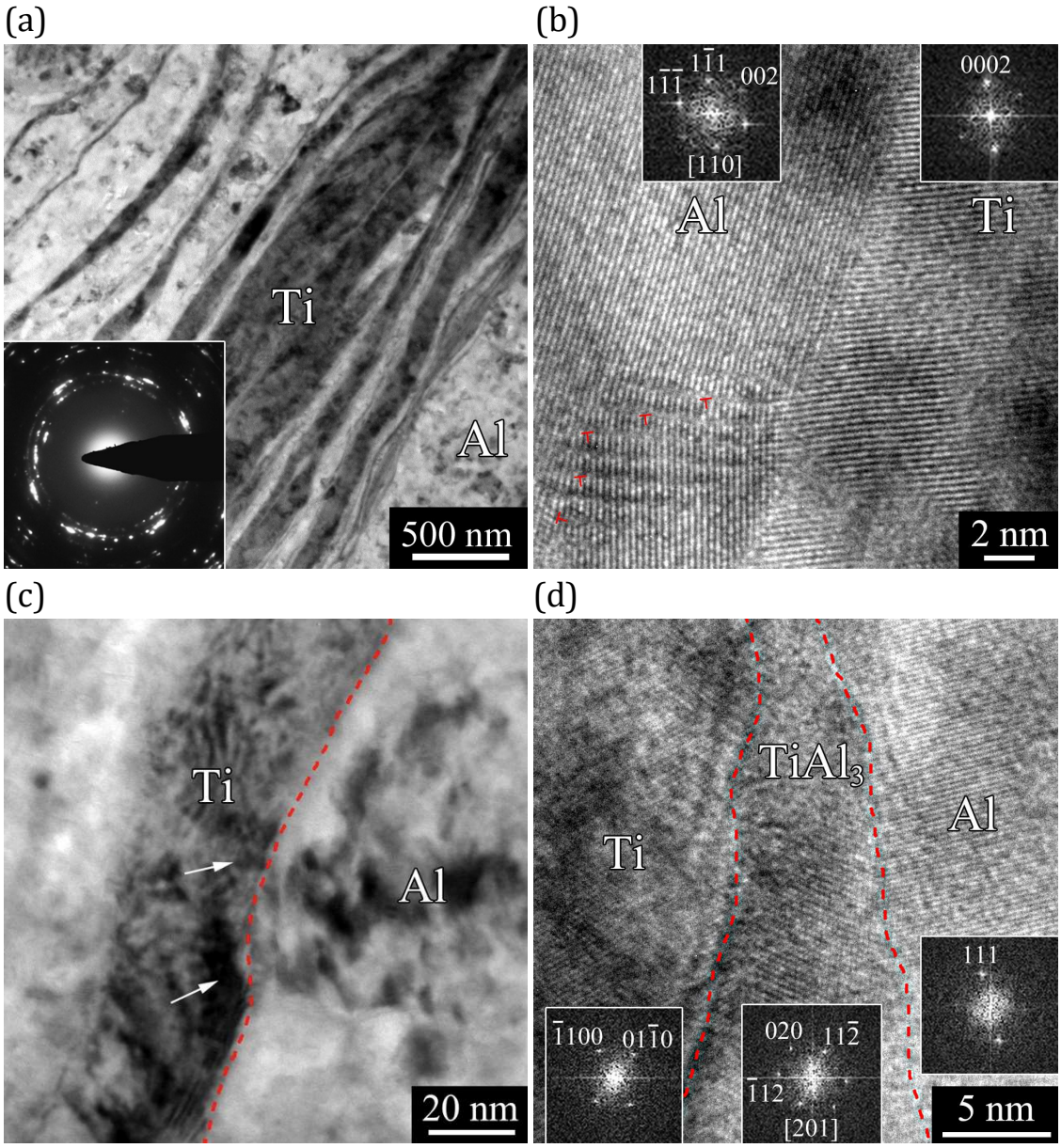

Figure 5. (a) Bright field TEM micrograph and the SAED pattern (inset) of the Al/Ti lamellas in γ58 FIB lifted TEM sample. (b) HRTEM of the coherent Al/Ti interphase boundary in the γ58 sample and the corresponding FFT patterns. (C) Bright field TEM and (d) HRTEM micrographs of the incoherent Al/Ti interphase boundary in the γ58 sample and the corresponding FFT patterns.

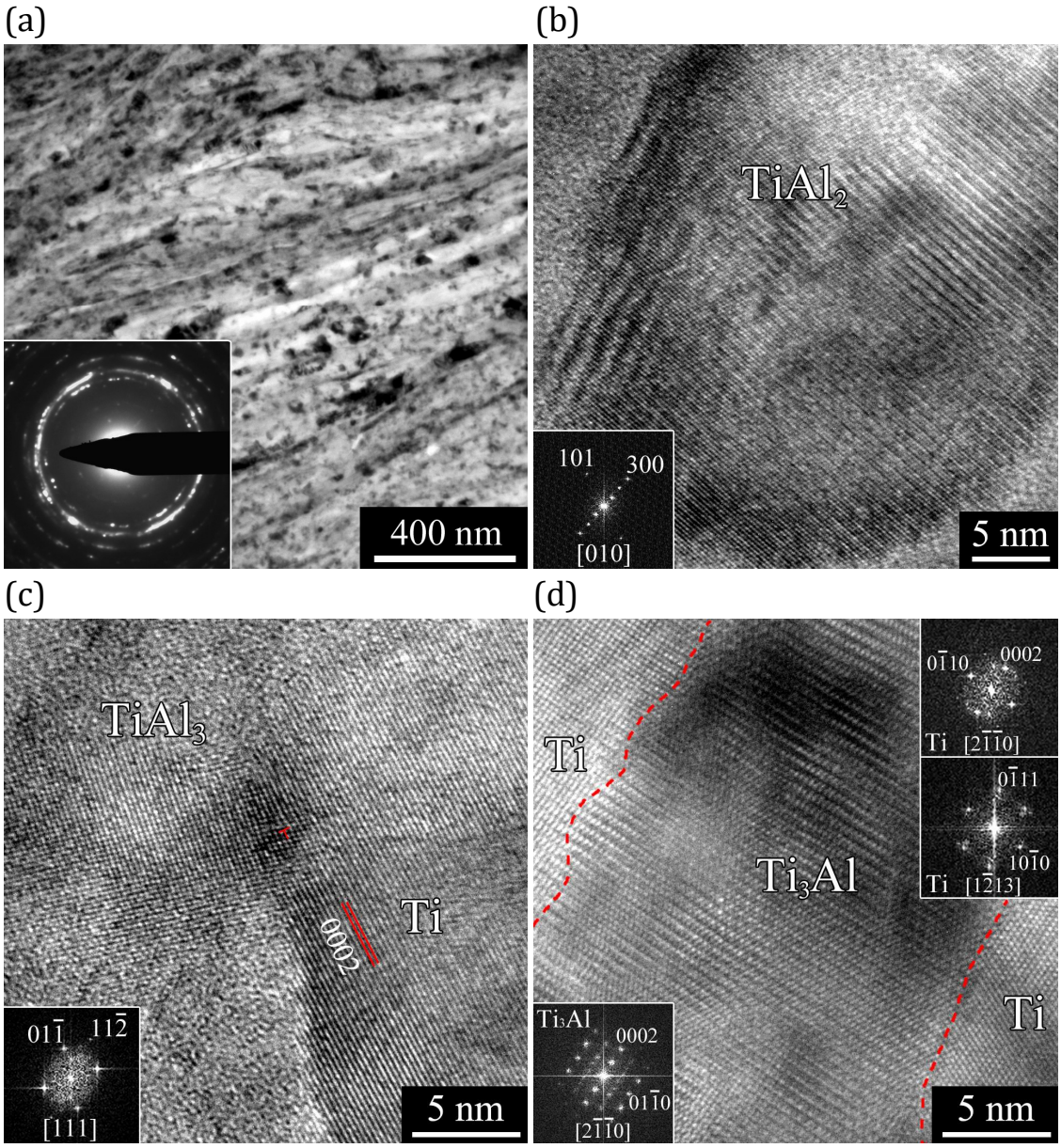

Figure 6. (a) Bright field TEM micrograph and the SAED pattern (inset) of the Al/Ti lamellas in the γ87 FIB lifted TEM sample. (b) HRTEM micrograph of $TiAl_2$ intermetallic phase formed in the γ87 sample and the corresponding FFT pattern. (c) HRTEM micrograph of $TiAl_3$ intermetallic compound formed in the γ87 sample and the corresponding FFT pattern. (d) HRTEM micrograph of the Ti_3Al intermetallic compound formed in the γ87 sample and the corresponding FFT patterns.